Comparative Study on the Organic Solvent of IrO₂–Ionomer Inks used for Spray Coating of Anode for Proton Exchange Membrane Water Electrolysis

Hye Young Jung[1,2], Yongseok Jun[2], Kwan-Young Lee[3], Hyun S. Park[1,4,5]*, Sung Ki Cho[1]*, and Jong Hyun Jang[1,2,4]*

[1]*Hydrogen·Fuel Cell Research Center, Korea Institute of Science and Technology (KIST), Seoul 02792, Republic of Korea*
[2]*Graduate School of Energy and Environment, KU-KIST Green School, Korea University, Seoul 02481, Republic of Korea*
[3]*Department of Chemical and Biological Engineering, Korea University, Seoul 02841, Republic of Korea*
[4]*Division of Energy & Environment Technology, KIST School, University of Science and Technology (UST), Seoul 02792, Republic of Korea*
[5]*KHU-KIST Department of Converging Science and Technology, Kyung Hee University, Seoul 02447, Republic of Korea*

ABSTRACT

Currently, spray coating has attracted interest in the mass production of anode catalyst layers for proton exchange membrane water electrolysis (PEMWE). The solvent in the spray ink is a critical factor for the catalyst dispersion in ink, the microstructure of the catalyst layer, and the PEMWE performance. Herein, various pure organic solvents were examined as a substitute for conventional isopropanol-deionized water (IPA-DIW) mixture for ink solvent. Among the polar solvents that exhibited better IrO₂ dispersion over nonpolar solvents, 2-butanol (2-BuOH) was selected as a suitable candidate. The PEMWE single cells were fabricated using 2-BuOH at various ionomer contents, spray nozzle types, and drying temperatures, and their performance was compared to the cells fabricated using a conventional IPA-DIW mixture. The PEMWE single cells with 2-BuOH solvent showed good performances comparable to the conventional IPA-DIW mixture case and highly durable performances under accelerated degradation tests.

1. Introduction

To meet the 1.5ºC target of global warming along with net zero emissions realized by energy transformation from fossil fuels to renewable energy, the utilization of hydrogen as a renewable energy carrier is required [1-3]. Hydrogen has been mainly produced from fossil fuels using steam methane reforming, which accounts for approximately 96% of the total hydrogen production [4]. Accordingly, water electrolysis using renewable electrical energy is urgently required for clean hydrogen production and the long-term storage of surplus electricity generated from solar and wind power units [5]. Among the various types of water electrolysis processes, proton exchange membrane water electrolysis (PEMWE) is the most suitable for clean hydrogen production because of its high current density, good load-following capability, fast response time, and compact size [6]. According to the International Energy Agency (IEA) report, "Net Zero Emissions by 2050 Scenario", the demand for water electrolysis cell deployment is expected to reach 3,600 GW by 2050 [7]. However, for the full commercialization of PEMWE, further research and development focused on the scale-up (*e.g.*, electrode area), automation, and fast production of water electrolysis cells are required to reduce material and manufacturing costs [7]. Therefore, it is necessary to develop fabrication techniques

suitable for the mass production of PEMWE systems.

In PEMWE system, IrO_2-based anode is one of the key components closely related to the performance of electrolysis cell, and various catalyst coating methods have been investigated: slot-die coating [8,9], spray coating [10-17], electrodeposition [18-21], sputtering [22], reactive spray deposition [23], atomic layer deposition [24], doctor blade coating [25,26], inkjet printing [27,28], impregnation–reduction [29], and so on. For mass production, the slot-die coating combined with roll-to-roll process, which has a high production rate [8,9], has been extensively developed by PEMWE companies such as Plug Power and NEL Hydrogen [30,31], while further improvement in the uniformity of the coated film [31,32] and the membrane swelling problem due to the long interaction time between the ink solvent and the membrane [8] are required for enhanced performances. In contrast, the spray coating technique can provide a high uniformity of coated layer, less vulnerability to membrane swelling, precise control of catalyst loading, and good scalability of coating area [8], even though its production rate is relatively low compared to the conventional slot-die coating. Also, the electrodeposition, where the catalyst precursors are directly transformed to the catalyst layers mainly on conductive porous transport layers (PTLs), is also expected to be an alternative technology for the mass production as it was reported to provide high performance [18,20,21], scalability, and the precise control of the catalyst loading amount.

For the spray coating, there have been various studies to enhance the performances, including the effect of catalyst ink characteristics and spray conditions. Ink is a primary component for spray coating and composed of IrO_2 powder, ionomer (Nafion resin), and solvent, which is usually the mixture of organic solvents and deionized water, such as isopropanol and deionized water (IPA-DIW) [11,13,15-17] or *n*-propanol and DIW [10,12,14]. These recipes have also been commonly used for the spray coating of the catalyst layer in proton exchange membrane fuel cells owing to the good dispersion of catalyst particles in the ink and fast evaporation after spraying [33-35]. However, some issues have been reported for the propanol/water mixture solvents: the swelling and deformation of the Nafion membrane [8,9,36], and the formation of the rough catalyst layer during the evaporation of solvents [37]. Some studies

reported that the fuel cell fabricated by using pure organic solvents such as ethylene glycol and dimethyl oxalate, instead of using the conventional mixture, exhibited superior performance with changing of the catalyst microstructure, which led to the enhanced mass transport of the reactant [38,39]. Although all of ink components, including solvent in spray coating, affect the performance of water electrolysis cells [12], the use of pure organic solvent for spray coating has not been attempted for the fabrication of water electrolysis cells. Our study focused on the use of pure organic solvents for spray coating of the catalyst layer for water electrolysis cells. The use of the pure organic solvent should be investigated in various aspects, such as the catalyst dispersion in the solvent, spray-feasibility, and electrolysis performance. In this study, various pure organic solvents were examined as substitutes for IPA-DIW in the catalyst ink of spray coating for the fabrication of the anode of the PEMWE electrolysis cell. Firstly, the dispersion characteristics of several pure organic solvents were examined, and then the selected solvent was further examined by single-cell tests in comparison to the conventional IPA-DIW mixture solvent case. In addition, various spray conditions, such as ionomer concentration, drying temperature, and spray nozzle type were optimized for the PEMWE performances.

2. Experimental

2.1 Catalyst ink preparation and characterization

An IrO_2 powder (Alfa Aesar, Premion®, metal trace 99.99%, Ir 84.5%, 43396) and Nafion resin solution (Sigma-Aldrich) were purchased as commercial-grade chemicals. The tested solvents were IPA (Samchun Chemical), 2-BuOH (Samchun Chemical), acetonitrile (MeCN; Sigma-Aldrich), 1,1,1,3,3,3-hexafluoro-isopropanol (HFIPA; Sigma-Aldrich), toluene (Sigma-Aldrich), hexane (Sigma-Aldrich), benzene (Sigma-Aldrich), and deionized water (DIW, >18 MΩ). The IrO_2 powder (10 mg mL^{-1}) and ionomer (0.53 mg mL^{-1} which corresponds to 5 wt.% of IrO_2) were dispersed in each solvent under magnetic stirring for 1 h and then ultrasonicated in an ice water bath for ~30 min.

The size and ζ-potential of the dispersed particles were analyzed through dynamic light scattering (DLS; ELSZ-2000ZS, Photal Otsuka Electronics,

664.5 nm), and the Z-average diameter of the particles was measured five times for each ink. For DLS measurements, 0.5 mg mL^{-1} IrO$_2$ dispersions and 0.53 mg mL^{-1} Nafion ionomer dispersions were utilized to ensure light transmittance. Before DLS measurements, the prepared inks were microfiltered to eliminate large particles, which can lead to false scattering peaks. To confirm the measurement error, monodisperse (0.10±0.03 µm) polystyrene particles (Supelco$^®$) were used as the standard sample for DLS analyses, and the size deviation was determined to be below 5%. The ζ-potentials of various inks were measured using a slit cell.

2.2 Electrode and MEA fabrication

The anode catalyst inks were prepared by dispersing the IrO$_2$ powder and a Nafion resin solution (5 wt.% solution, Sigma-Aldrich) in 2-BuOH or 1:1 IPA-DIW mixture as the solvent. The amount of the catalyst was 10 mg mL^{-1} (which corresponds to 1 wt.% of the total solvent). The anode ink solution was first moderately stirred using a magnetic bar and then ultrasonicated for 30 min in an ice bath. Then, the anode catalyst ink was sprayed onto Nafion 212 (Chemours, 51 µm thick) membranes at a mantle temperature of 90–120°C using a dual concentric air nozzle (NNC-DN-1823, 18-23G, NanoNC) for conventional spray coating or an ultrasonic nozzle (Sono-Tek, AccuMist$^®$ 120 kHz, 30 mL h^{-1}) for ultrasonic spray coating. After spray coating the catalyst ink, the MEA was heated on a hot plate for 30 min to evaporate the residual solvent. The loading of the IrO$_2$ catalyst was controlled at 1.0 mg cm^{-2} by measuring the sprayed amount using a microbalance (Entris 2241-1S).

2.3 Electrochemical characterization of single cells

Electrochemical measurements were conducted on single cells with a geometric electrode area of 4.0 cm^2 consisting of a Ti anode plate, a graphite cathode, and bipolar plate (CNL Energy). All electrochemical measurements were conducted using a potentiostat (Biologic HCP-803). Linear sweep voltammetry (LSV) was conducted in the voltage range of 1.20–2.0 V at a scan rate of 10 mV s^{-1}. The impedance spectra were recorded with an amplitude of 18 mV over the frequency range of 50 mHz to 30 kHz in the potentiostatic mode at 1.90 V. Accelerated degradation tests (ADTs) were performed by applying tri-

angular voltage between 1.60 and 1.90 V at a scan rate of 300 mV s^{-1} for 8000 cycles. After ADT, LSV and EIS data were acquired to investigate the electrochemical degradation of the MEA.

2.4 Catalyst layer characterization

The porosity of the catalyst layer was measured using mercury intrusion porosimetry (Autosorb-iQ 2ST/MP, Quanthrome, PM33GT). Samples were prepared by spraying the same ink onto a 4.0 cm^2 spray mask fixed on a vacuum hot plate. After the spraying was completed, the 4.0 cm^2 anode was sliced into four 1.0 cm^2 specimens for repeated measurements. The intrusion pressure ranged from 0.2 to 32982.8 PSIA (absolute pressure) in all tests. The morphology of the catalyst layer was observed using field-emission scanning electron microscopy (FE-SEM; Inspect F50), and the cross-sectional images were scanned using a focused ion beam (FIB; Helios NanoLab 600).

3. Results and Discussion

3.1 Dispersion of the catalyst in various organic solvents

Among the various inexpensive and readily available organic solvents considering the application for the mass production of anode catalyst layer, six organic solvents (polar: 2-BuOH, HFIPA, and MeCN / nonpolar: hexane, benzene, and toluene) having various dielectric constants in the range of 1 to 50 (where the dielectric constant of IPA-DIW is 47.3) were selected and the dispersion characteristics of the IrO$_2$ catalyst powder in these solvents were examined through DLS measurements (Fig. 1). The polar solvents with higher dielectric constants exhibited good IrO$_2$ dispersion characteristics, and the size of the dispersed particles was below 400 nm. On the other hand, the particle size reached the micrometer-scale in nonpolar solvents, indicating poor dispersibility of the catalyst. Among the polar solvents with good IrO$_2$ dispersion, the 2-BuOH was selected as a suitable candidate for replacing the conventional IPA-DIW mixture. Other polar solvents have disadvantages for spray coating in large scale: the MeCN is highly volatile and toxic [40] and was also reported to degrade the catalytic activity and proton conductivity in proton exchange membrane [41]; and HFIPA is also toxic [42] and relatively expensive.
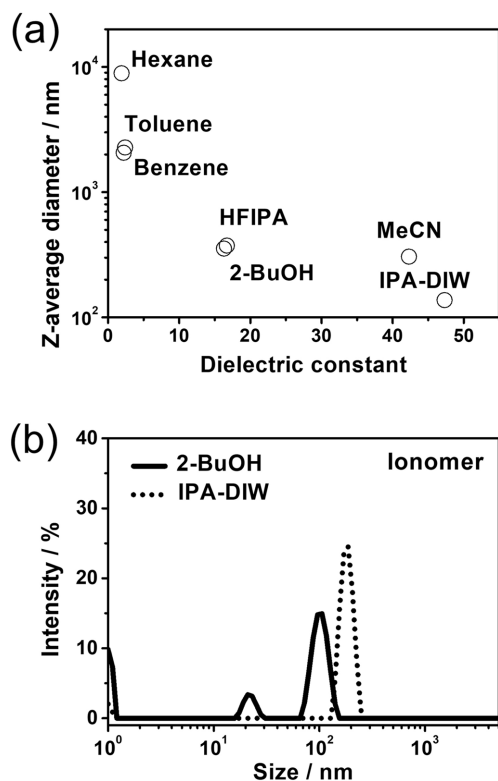
Fig. 1. Dispersion properties of neat IrO$_2$ and ionomer in 2-BuOH and IPA-DIW solvent. (a) IrO$_2$ dispersion size (Z-average diameter) of IrO$_2$ dispersed in various solvents, and (b) DLS spectra of ionomer dispersed in 2-BuOH and IPA-DIW. All inks were diluted to acquire the stable DLS spectra.
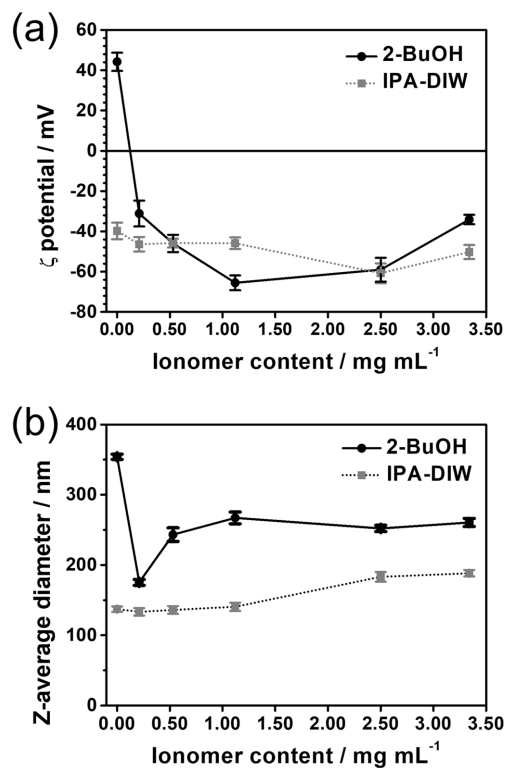

Fig. 2. Dispersion properties of IrO$_2$-ionomer in 2-BuOH and IPA-DIW solvent with respect to ionomer content as 0, 0.21, 0.53, 1.12, 2.50, and 3.34 mg mL^{-1}. (a) ζ-potential and (b) dispersion size (Z-average diameter) of IrO$_2$-ionomer agglomerate in 2-BuOH and IPA-DIW solvent containing various ionomer content. All inks were diluted adequately to acquire the DLS spectra.

Next, the dispersibility of the ionomer in 2-BuOH and IPA-DIW was also evaluated via DLS measurements (Fig. 1). The Nafion ionomer in 2-BuOH displayed a major peak at 106 nm with a relative intensity of 71%, accompanied by minor peaks at 1 and 25 nm. In the case of Nafion in IPA-DIW, a major peak appeared at 187 nm with a minor peak at 1 nm, which is in reasonable agreement with previous studies [43]. Therefore, it could be confirmed that the 2-BuOH can provide good ionomer dispersion similar to the IPA-DIW mixture.

Fig. 2a shows the ζ-potentials of the IrO$_2$ catalyst (0.5 mg mL^{-1}) dispersed in 2-BuOH and IPA-DIW as a function of the ionomer content. It indicates that the addition of a small amount of the ionomer (0.21 mg mL^{-1}) to the catalyst suspension in 2-BuOH resulted in a high ζ-potential (>|30| mV) which would lead to

appropriate dispersion of the catalyst. In 2-BuOH, the ζ-potential of the IrO$_2$ catalyst was 46.4 mV without the ionomer. However, it decreased substantially to -31.13 mV with the addition of 0.21 mg mL^{-1} ionomer, and the negative value was maintained (-34 to -66 mV) with a further increase in the ionomer content in the ink. This result implies that the surface of IrO$_2$ particles, which is initially positively charged in pure 2-BuOH, can be readily covered with the ionomer, as similarly observed for the IrO$_2$ particles in *n*-propanol [44]. Meanwhile, the ζ-potential of the IrO$_2$ particles in IPA-DIW ranged from -39.78 to -60.79 mV, and it did not change significantly with the addition of the ionomer.

Fig. 2b plots the Z-average diameter of the IrO$_2$–ionomer colloids in 2-BuOH and IPA-DIW against the ionomer contents, and the results reveal that the

diameter of the colloidal particles in 2-BuOH was slightly larger than that in IPA-DIW. In the case of 2-BuOH, the Z-average diameter was ~350 nm in the absence of the ionomer, and it sharply decreased to 170 nm with the addition of 0.21 mg mL^{-1} ionomer. This could be attributed to the change in the ζ-potential of the dispersed catalyst particles, as shown in Fig. 2a. The colloidal size increased to ~250 nm with the further addition of the ionomer, indicating that the excess ionomer stacked on the colloid surface, leading to large catalyst agglomerates. The Z-average diameter of the IrO$_2$–ionomer colloidal particles in the IPA-DIW was smaller than that of 2-BuOH over the entire range of the ionomer content investigated in this study, possibly due to the difference in acidity of solvents.

3.2 Performances of single cells with anodes fabricated using the 2-BuOH-based ink

Anodes were fabricated using 2-BuOH as the solvent of the IrO$_2$–ionomer ink, and their performances in PEMWE were evaluated and compared with those of the anodes fabricated using IPA-DIW (Fig. 3). In the case of conventional spray coating, the performance of the single cell with the anode fabricated using 2-BuOH was slightly inferior to that of the cell with the anode fabricated using IPA-DIW (Fig. 3a). At a cell voltage of 1.90 V, the current densities of the anodes fabricated with 2-BuOH and IPA-DIW were 4.7 and 5.9 A cm^{-2}, respectively. However, when the ultrasonic spray coating technique was utilized, the PEMWE performance of the anode fabricated using 2-BuOH was enhanced larger compared to the IPA-DIW case, and it exhibited a current density of 5.7 A cm^{-2} at 1.90 V, which corresponds to 92% of that of the IPA-DIW. It suggests that the effect of ultrasonic atomization was dependent on the solvent type. For 2-BuOH and IPA-DIW mixture solvents, the effect of other experimental variables, such as ionomer content and drying temperature, was further examined by PEMWE single-cell tests.

Fig. 4a and 4b present the PEMWE performance of the systems fabricated with the ultrasonic spray coating using catalyst inks containing various ionomer contents. The highest PEMWE performance was observed at 0.53 mg mL^{-1} ionomer content in the ink for both the 2-BuOH and IPA-DIW cases, which is comparable to that of the previously reported *n*-propanol-DIW solvent case [12] As shown in Fig. 4c,
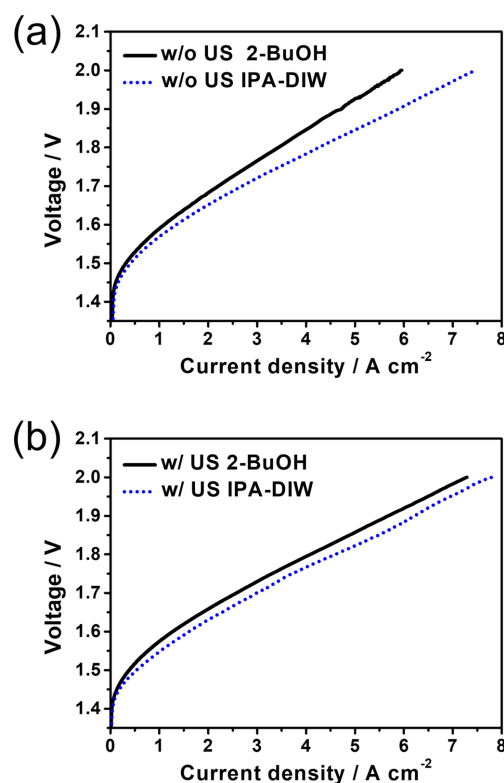

Fig. 3. Effect of ultrasonic spray coating on the water electrolysis cell performance. Polarization curves measured from water electrolysis cell prepared with 2-BuOH and IPA-DIW ink (a) using the conventional spray coating (denoted as w/o US) and (b) using the ultrasonic spray (denoted as w/ US).

the electrolysis cell performance decreased as the ionomer content increased beyond 2.50 mg mL^{-1} because of the blockage of the active catalytic sites by the excess ionomer [16]. The current density decreased more drastically at higher voltages, implying that the decrease in the electrical conductivity and mass transport due to the overload of the ionomer can affect the cell performance more severely than the insufficient ionic conductivity at a relatively low ionomer content. At a low applied voltage (1.66 V), where the effects of the reaction kinetics and active surface area are more dominant compared to those at high cell voltages, the performances of the electrolysis cells were comparable for the two ink cases. As shown in Fig. 4d, the charge transfer resistance for the 2-BuOH case was slightly larger than that of the IPA-DIW case, consistent with the performance
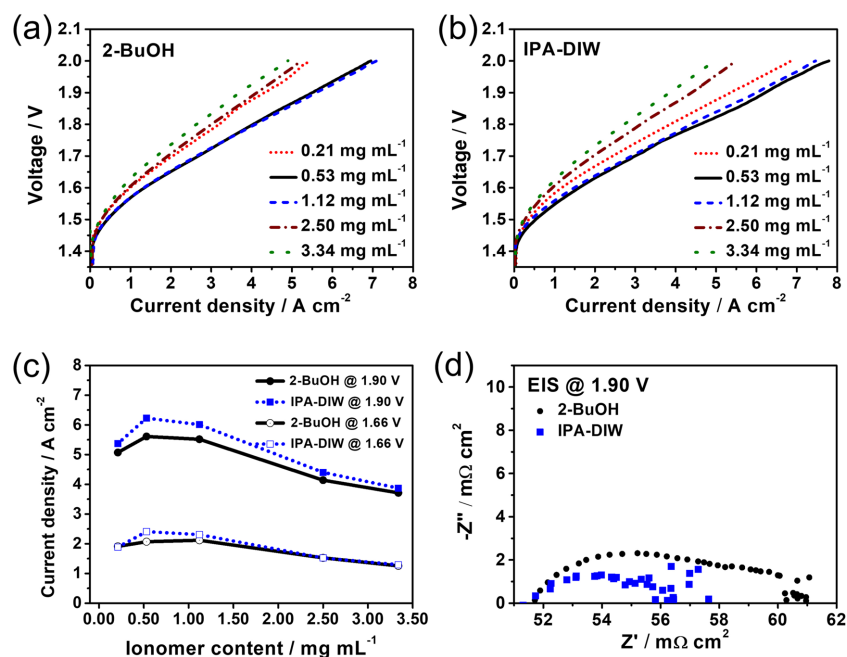
Fig. 4. Electrochemical performances of water electrolysis cell fabricated using ultrasonic spray coating with 2-BuOH and IPA-DIW ink containing various ionomer content; (a) polarization curve from 2-BuOH ink with various ionomer content, (b) polarization curve from IPA-DIW ink with various ionomer content, (c) current density performances at 1.66 V and 1.90 V in each 2-BuOH and IPA-DIW solvent with respect to ionomer contents, (d) Nyquist plots from EIS measurement at 1.90 V. (ultrasonic spraying condition: 30 mL h^{-1}, 110°C at the ultrasonic nozzle).
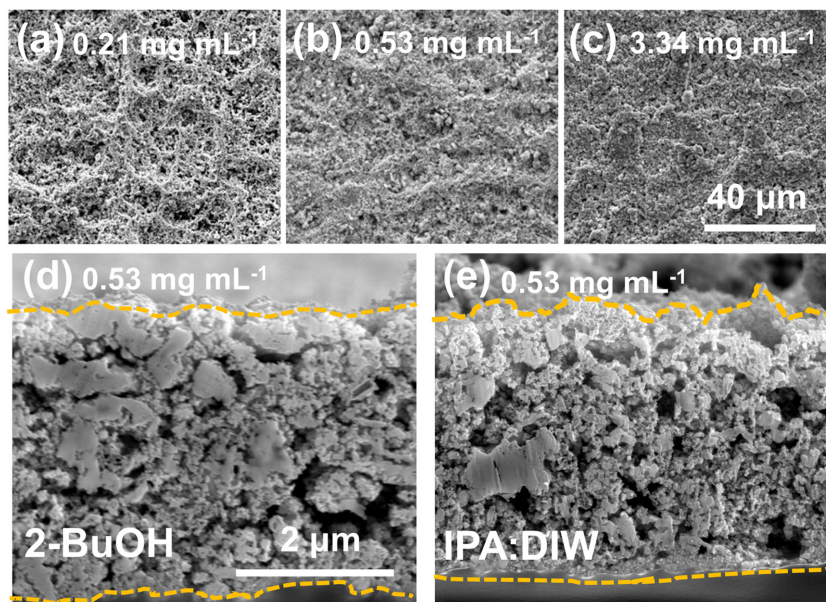

Fig. 5. Surface and cross-sectional images of IrO$_2$ catalyst layer coated with ultrasonic spray using 2-BuOH ink with (a) 0.21, (b) 0.53, (c) 3.34 mg mL^{-1} ionomer content. (d,e) Cross-sectional FIB images of IrO$_2$ catalyst layer prepared with using (d) 2-BuOH and (e) IPA-DIW solvent (ultrasonic spraying condition: 30 mL h^{-1}, ionomer content: 0.53 mg mL^{-1}, drying temperature: 110°C).

results presented in Fig. 4c.

Fig. 5 shows the surface and cross-sectional SEM images of the IrO_2 catalyst layer prepared using the 2-BuOH ink. As expected, the film fabricated with a low ionomer content exhibited a more porous and cracked surface (Fig. 5a–c). It also showed that the thicknesses of the catalyst layers coated from 2-BuOH and IPA-DIW were almost the same (Fig. 5d,e), which is consistent with the controlled loading amounts of IrO_2 and ionomer in 2-BuOH and IPA-DIW. However, the catalyst layer coated from 2-BuOH had more agglomerated and coarse particles compared to IPA-DIW, which might increase the heterogeneity of the microstructure [45].

3.4 Effect of drying temperature for 2-BuOH and IPA-DIW inks

The effect of the ink drying temperature on the single-cell performance was investigated by analyzing the polarization curves (Fig. 6a,b). Specifically, the current density at 1.90 V from the polarization curve was plotted against the drying temperature (Fig. 6c). For both the 2-BuOH (Fig. 6a) and IPA-DIW (Fig. 6b) cases, the PEMWE performance increased with the drying temperature and reached a maximum at 110°C. Rapid solvent evaporation using a high drying temperature would be beneficial for obtaining a more uniform microstructure as it limits ionomer migration [46] and prevents uneven swelling of the Nafion membrane [8]. However, the PEMWE performance of the anode dried at 120°C was lower than that of the anode dried at 110°C possibly because of the deformation of the membrane annealed near its T_g (~120°C) and reduced rehydration [47]. The effect of drying temperature was less drastic for 2-BuOH compared to IPW-DIW, which might be related to the difference in the boiling temperatures of 2-BuOH (99.5°C) and IPA-DIW (80.4°C). These characteristics of 2-BuOH can be beneficial for the large-scale processes with temperature variations.

Fig. 7a and 7b present the pore size and volume fraction of the catalyst layers prepared using the 2-BuOH and IPA-DIW inks with 0.53 mg mL^{-1} ionomer content, as evaluated by mercury porosimetry. At the same drying temperature, the total pore volume of the catalyst layer prepared from the 2-BuOH ink was half of that obtained from the IPA-DIW ink. This tendency might be because of the heterogeneity of the ionomer size in BuOH (Fig. 1b), as it might block the
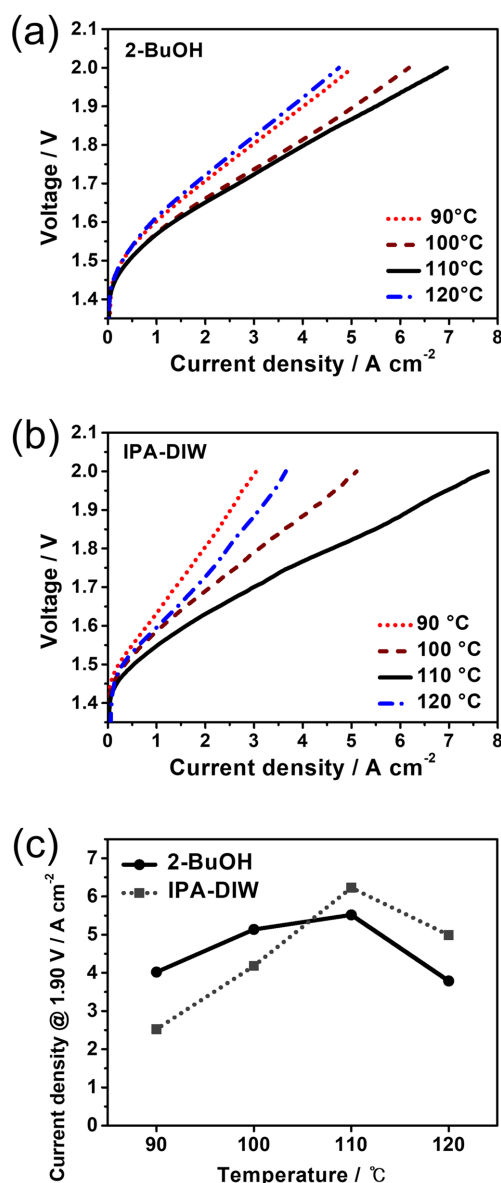

Fig. 6. Electrochemical performances of water electrolysis cell fabricated using ultrasonic spray coating with various drying temperature (a) Polarization curve from 2-BuOH ink, (b) Polarization curve from IPA-DIW ink, and (c) the plot of current density at 1.90 V from polarization curves(a) and (b) along with the drying temperature. The geometric area of MEAs were 4.0 cm^2 in all experiments.

pore effectively. For both solvent cases, the total pore volume of the catalyst layer processed at 110°C was higher than that of the layer processed at 90°C, which could be the reason for the better performances of the
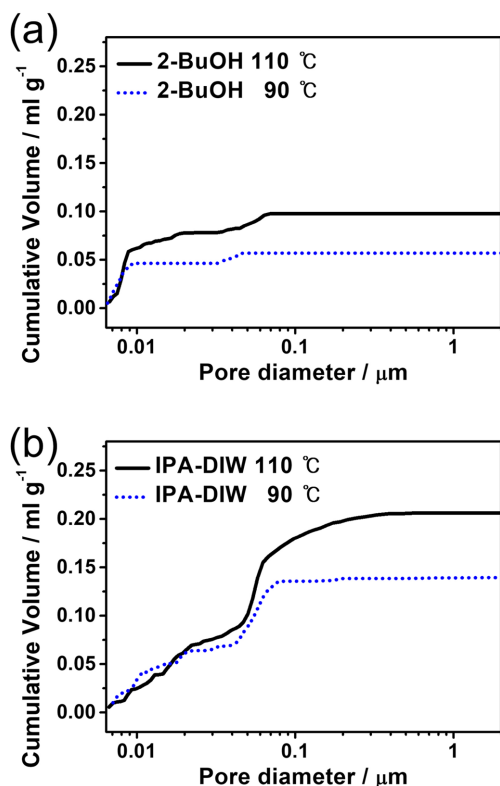
Fig. 7. Total cumulative pore volume from mercury intrusion porosimetry measurement on IrO_2 anode catalyst layer prepared with (a) 2-BuOH ink or (b) IPA-DIW ink containing 0.53 mg mL^{-1} ionomer (ultrasonic spraying condition: 30 mL h^{-1}, drying temperature: 90 or 110°C).
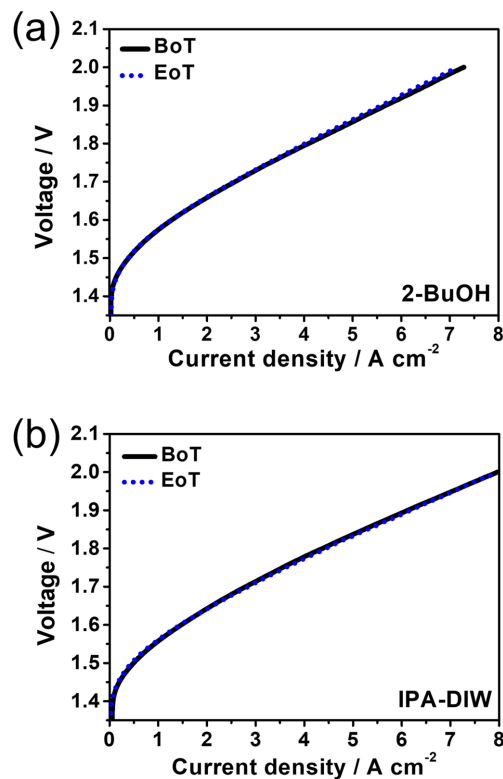

Fig. 8. ADT results of catalyst layers prepared from 2-BuOH and IPA-DIW, obtained with triangular voltage cycling as 8000 times with 300 mV s^{-1} from 1.60 V to 1.90 V. Polarization curve of (a) 2-BuOH condition and (b) IPA-DIW condition at the beginning of the test (BoT) and the end of the test (EoT).

electrolysis cells with the anodes dried at 110°C. Notably, in the catalyst layer obtained from the 2-BuOH ink, pores smaller than 10 nm developed more intensely than in the IPA-DIW case. This result might be because the larger particles in 2-BuOH ink (250 nm at 0.53 mg mL^{-1} ionomer content, Fig. 2b) generated higher number of nanosized gaps between the agglomerated particles compared to the particles in IPA-DIW ink (140 nm).

3.5 ADT for evaluating the electrolysis cell durability

Fig. 8 shows the polarization curves before and after ADT for the MEAs fabricated using 2-BuOH and IPA-DIW inks. After ADT, where triangular voltage scans between 1.60 and 1.90 V were repeated 8000 times, the voltage change at 5.0 A cm^{-2} was less than 0.5%, indicating that the PEMWE performance was stably maintained under harsh conditions for both 2-BuOH and IPA-DIW solvent.

4. Conclusions

In summary, this study presented pure 2-BuOH as a substitute solvent of spraying ink containing IrO_2–ionomer colloids for the fabrication of PEMWE anodes. In the catalyst ink with 2-BuOH, the IrO_2–ionomer agglomerate size was twice as large as that in the IPA-DIW ink at 0.53 mg mL^{-1} ionomer content, and the inks with both the solvents presented a stable dispersion of the colloids with a ζ-potential of approximately -40 mV at ionomer contents of 0.21–3.34 mg mL^{-1}. The electrolysis cell fabricated using the 2-BuOH ink exhibited a current density of 5.7 A cm^{-2} at 1.90 V, which is ~92% of that of the electrol-

ysis cell fabricated using the IPA-DIW-based ink. This study demonstrates that pure 2-BuOH is a suitable solvent for spray coating the catalyst layer in the manufacturing of PEMWE systems.

Acknowledgments

References

[1] International Energy Agency (IEA), *Global Hydrogen Review 2021*, IEA, Paris, France, **2021**.

[2] W. Hwang and Y.-E. Sung, *J. Electrochem. Sci. Technol.*, **2023**, *14(2)*, 120-130.

[3] A. Lim, M. K. Cho, S. Y. Lee, H.-J. Kim, S. J. Yoo, Y.-E. Sung, J. H. Jang, and H. S. Park, *J. Electrochem. Sci. Techol.*, **2017**, *8(4)*, 265-273.

[4] K. Ayers, N. Danilovic, R. Ouimet, M. Carmo, B. Pivovar, and M. Bornstein, *Annu. Rev. Chem. Biomol. Eng.*, **2019**, *10*, 219-239.

[5] S. E. Hosseini, and M. A. Wahid, *Renew. Sustain. Energy Rev.*, **2016**, *57*, 850-866.

[6] C.-W. Sun and S.-S. Hsiau, *J. Electrochem. Sci. Technol.*, **2018**, *9(2)*, 99-108.

[7] A. Mayyas, M. Ruth, B. Pivovar, G. Bender, and K. Wipke, *Manufacturing cost analysis for proton exchange membrane water electrolyzers*, National Renewable Energy Laboratory, Golden, CO, United States, **2019**, NREL/TP-6A20-72740.

[8] J. Park, Z. Kang, G. Bender, M. Ulsh, and S. A. Mauger, *J. Power Sources*, **2020**, *479*, 228819.

[9] A. Steinbach, *Low-Cost, High Performance Catalyst Coated Membranes for PEM Water Electrolyzers*, 3M Company, Maplewood, MN, United States, **2022**, DOE-3M-0008425

[10] S. M. Alia, M.-A. Ha, G. C. Anderson, C. Ngo, S. Pylypenko, and R. E. Larsen, *J. Electrochem. Soc.*, **2019**, *166(15)*, F1243-F1252.

[11] M. Bühler, F. Hegge, P. Holzapfel, M. Bierling, M. Suermann, S. Vierrath, and S. Thiele, *J. Mater. Chem. A*, **2019**, *7(47)*, 26984-26995.

[12] S. M. Alia, K. S. Reeves, J. S. Baxter, and D. A. Cullen, *J. Electrochem. Soc.*, **2020**, *167*, 144512.

[13] P. K. R. Holzapfel, M. Bühler, D. Escalera-López, M. Bierling, F. D. Speck, K. J. J. Mayrhofer, S. Cherevko, C. V. Pham, and S. Thiele, *Small*, **2020**, *16(37)*, 2003161.

[14] J. Lopata, Z. Kang, J. Young, G. Bender, J. W. Weidner, and S. Shimpalee, *J. Electrochem. Soc.*, **2020**, *167*, 064507.

[15] B. Mayerhöfer, D. McLaughlin, T. Böhm, M. Hegelheimer, D. Seeberger, and S. Thiele, *ACS Appl. Energy Mater.*, **2020**, *3(10)*, 9635-9644.

[16] Y. Jang, C. Seol, S. M. Kim, and S. Jang, *Int. J. Hydrog. Energy*, **2022**, *47(42)*, 18229-18239.

[17] A. Voronova, H.-J. Kim, J. H. Jang, H.-Y. Park, and B. Seo, *Int. J. Energy Res.*, **2022**, *46(9)*, 11867-11878.

[18] B.-S. Lee, S. H. Ahn, H.-Y. Park, I. Choi, S. J. Yoo, H.-J. Kim, D. Henkensmeier, J. Y. Kim, S. Park, S. W. Nam, K.-Y. Lee, and J. H. Jang, *Appl. Catal. B: Environ.*, **2015**, *179*, 285-291.

[19] S. Choe, B.-S. Lee, and J. H. Jang, *J. Electrochem. Sci. Technol.*, **2017**, *8(1)*, 7-14.

[20] S. Choe, B.-S. Lee, M. K. Cho, H.-J. Kim, D. Henkensmeier, S. J. Yoo, J. Y. Kim, S. Y. Lee, H. S. Park, and J. H. Jang, *Appl. Catal. B: Environ.*, **2018**, *226*, 289-294.

[21] A. Lim, J. Kim, H. J. Lee, H.-J. Kim, S.J. Yoo, J. H. Jang, H.-Y. Park, Y.-E. Sung, and H. S. Park, *Appl. Catal. B: Environ.*, **2020**, *272*, 118955.

[22] E. Slavcheva, I. Radev, S. Bliznakov, G. Topalov, P. Andreev, and E. Budevski, *Electrochim. Acta*, **2007**, *52(12)*, 3889-3894.

[23] K. E. Ayers, J. N. Renner, N. Danilovic, J. X. Wang, Y. Zhang, R. Maric, and H. Yu, *Catal. Today*, **2016**, *262*, 121-132.

[24] A. Laube, A. Hofer, S. Ressel, A. Chica, J. Bachmann, and T. Struckmann, *Int. J. Hydrog. Energy*, **2021**, *46(79)*, 38972-38982.

[25] C. Liu, M. Carmo, G. Bender, A. Everwand, T. Lickert, J. L. Young, T. Smolinka, D. Stolten, and W. Lehnert, *Electrochem. Commun.*, **2018**, *97*, 96-99.

[26] H.-J. Ban, M. Y. Kim, D. Kim, J. Lim, T. W. Kim, C. Jeong, Y.-A. Kim, and H.-S. Kim, *J. Electrochem. Sci. Technol.*, **2019**, *10(1)*, 22-28.

[27] M. Mandal, A. Valls, N. Gangnus, and M. Secanell, *J. Electrochem. Soc.*, **2018**, *165(7)*, F543-F552.

[28] G. Yang, S. Yu, Z. Kang, Y. Li, G. Bender, B. S. Pivovar, J. B. Green Jr, D. A. Cullen, and F.-Y. Zhang, *Adv. Energy Mater.*, **2020**, *10(16)*, 1903871.

[29] P. Millet, M. Pineri, and R. Durand, *J. Appl. Electrochem.*, **1989**, *19*, 162-166.

[30] F. Yang, C. Lei, A. Griffith, R. Stone, and C. Mittelsteadt, Plug Power. Inc., *Proton exchange membrane water electrolyzer membrane electrode assembly*, United States patent US; **2022**, US20220243339A1.

[31] S. Mauger, *Roll to Roll (R2R) Manufacturing of Electrolysis Electrodes for Low Cost Hydrogen Production*, National Renewable Energy Laboratory, Golden, CO, United States, **2022**, NREL/TP-5900-83194.

[32] E. B. Creel, K. Tjiptowidjojo, J. A. Lee, K. M.

Livingston, P. R. Schunk, N. S. Bell, A. Serov, and D. L. Wood III, *J. Colloid Interface Sci.*, **2022**, *610*, 474-485.

[33] T. T. Ngo, T. L. Yu, and H.-L. Lin, *J. Power Sources*, **2013**, *225*, 293-303.

[34] T. V. Cleve, S. Khandavalli, A. Chowdhury, S. Medina, S. Pylypenko, M. Wang, K. L. More, N. Kariuki, D. J. Myers, A. Z. Weber, S. A. Mauger, M. Ulsh, and K. C. Neyerlin, *ACS Appl. Energy Mater.*, **2019**, *11(50)*, 46953-46964.

[35] A. Lim, J. S. Lee, S. Lee, S. Y. Lee, H. Kim, S. J. Yoo, J. H. Jang, Y.-E. Sung, and H. S. Park, *Appl. Catal. B: Environ.*, **2021**, *297*, 120458.

[36] Y. D. Yi and Y. C. Bae, *Polymer*, **2017**, *130*, 112-123.

[37] Y.-H. Huang, Y.-H. Hsu, and Y.-T. Pan, *ACS Appl. Energy Mater.*, **2022**, *5(3)*, 2890-2897.

[38] T.-H. Yang, Y.-G. Yoon, G.-G. Park, W.-Y. Lee, and C.-S. Kim, *J. Power Sources*, **2004**, *127(1-2)*, 230-233.

[39] J.-H. Park, M.-S. Shin, and J.-S. Park, *Electrochim. Acta*, **2021**, *391*, 138971.

[40] D. R. Joshi and N. Adhikari, *J. Pharm. Res. Int.*, **2019**, *28(3)*, 1-18.

[41] Y. Zhai and J. St-Pierre, *Appl. Energy*, **2019**, *242*, 239-247.

[42] T. Shimizu, E. Nogami, Y. Ito, K. Morikawa, M. Nagane, T. Yamashita, T. Ogawa, F. Kametani, H. Yagi, and N. Hachiya, *Neurochem. Res.*, **2021**, *46*, 2056-2065.

[43] C.-Y. Ahn, J. Ahn, S. Y. Kang, O.-H. Kim, D. W. Lee, J. H. Lee, J. G. Shim, C. H. Lee, Y.-H. Cho, and Y.-E. Sung, *Sci. Adv.*, **2020**, *6*, eaaw0870.

[44] S. Khandavalli, J. H. Park, N. N. Kariuki, S. F. Zaccarine, S. Pylypenko, D. J. Myers, M. Ulsh, and S. A. Mauger, *ACS Appl. Mater. Interfaces*, **2019**, *11(48)*, 45068-45079.

[45] M. B. Salvado, P. Schott, L. Guétaz, M. Gerard, T. David, and Y. Bultel, *J. Power Sources*, **2021**, *482*, 228893.

[46] J. Zhang, Y. Pei, W. Zhu, Y. Liu, Y. Yin, Y. Qin, and M. D. Guiver, *J. Power Sources*, **2021**, *484*, 229259.

[47] S. H. de Almeida and Y. Kawano, *J. Therm. Anal. Calorim.*, **1999**, *58*, 569-577.